Biophysical Chemistry 159 (2011) 247–256

Contents lists available at ScienceDirect

Biophysical Chemistry

journal homepage: http://www.elsevier.com/locate/biophyschem

The influence of the peptide bond on the conformation of amino acids: A theoretical and FT-IR matrix-isolation study of *N*-acetylproline

Bram Boeckx *, Riet Ramaekers, Guido Maes

Department of Chemistry, University of Leuven, Celestijnenlaan 200 F, B-3001 Leuven, Belgium

ARTICLE INFO

Article history:
Received 7 May 2011
Received in revised form 4 July 2011
Accepted 8 July 2011
Available online 20 July 2011

Keywords:
DFT
Frequency
N-acetylated amino acid
Infrared spectroscopy
MP2

ABSTRACT

A combined experimental matrix-isolation FT-IR and theoretical study has been performed to investigate the conformational behavior of N-acetylproline. The conformational landscape of N-acetylproline was explored using successively higher computational methods, i.e. HF, DFT(B3LYP) and finally MP2. The exploration resulted in 10 conformations with a relative energy difference smaller than 22 kJ.mol^{-1} at the HF/3-21G level of theory. These conformations led to six different conformations after DFT(B3LYP) optimizations. Further optimization at the MP2/6-31++G** level of theory resulted in the same six conformations, all of them with an energy difference smaller than 11.5 kJ.mol^{-1}. One conformation with an intramolecular H-bond was found which was energetically the most favorable conformation. The vibrational and thermodynamical features were calculated using the DFT and MP2 methodologies. In the experimental matrix-isolation FT-IR spectrum, the most stable conformation was dominant and at least two non-H-bonded conformations could be identified. An experimental rotamerization constant between the H-bonded and the other non-H-bonded conformations was estimated and appeared to agree reasonably well with the theoretical MP2 predictions. Some new spectral features of N-acetylproline compared to proline were discovered which might be used to discriminate between the acetylated and non-acetylated form.

1. Introduction

The structure of proteins is of huge importance to understand many biological processes. As an elementary building block of proteins, amino acids are among the most important biomolecules. Additionally they have an enormous impact on the structure and thermodynamic and vibrational properties of proteins. For this reason and because proteins are too huge to be subjected to an extensive high-level computational study, amino acids can be in the past used as model molecules for proteins. But in proteins amino acids are involved in a peptide bond. For a better understanding of the influence of the peptide bond on the conformational behavior of amino acids we are currently investigating a series of *N*-acetylated amino acids. The acetylation of the nitrogen atom models a peptide bond and therefore this system serves as model system for C-terminus amino acids in peptides [18,30,31].

A very suitable technique to study the conformational behavior of amino acids and related molecules is matrix-isolation FT-IR spectroscopy combined with theoretical calculations. Since matrix-isolation essentially involves isolated molecules in a matrix, this represents the gas phase and therefore the FT-IR spectra can be compared with theoretically predicted spectra. Similar to other amino acids, NAP has a significant number of internal rotational axes which results in large conformational flexibility. The existence of several nearly similar conformations which can be expected for the *N*-acetylproline (NAP) makes the interpretation of the spectra extremely complicated and therefore the combination of the experimental and theoretical study is absolutely necessary.

N-acetylproline is the *N*-acetylated derivate of proline, the only amino acid where the side chain is covalently bonded to the nitrogen atom of its backbone forming a five-membered pyrrolidine ring. This ring gives rise to an extra conformational feature namely, puckering up and down. In peptides the ring constrains the conformational flexibility of the $C^{ac}-N-C^{\alpha}-C^{ca}$ dihedral angle which leads to local backbone rigidity. This makes proline a breaker element in α-helices and β-sheets' polypeptides and favors the formation of polyproline helices. The formation of the cis-rotamer is more favored in proline (10–30%) than in other amino acids (0.1%). As a matter of fact the ratio of cis- and trans-rotamers along the peptide bond preceding prolines is an important structural parameter [27].

The neutral amino acid proline has been investigated in a combined matrix-isolation FT-IR and theoretical study [28]. In this study two conformations with a different H-bond (N…HO and NH…O═C) could be identified in the low temperature matrix.

The cis/trans interconversion of *N*-acetyl-proline has been studied in small peptide models by a combined DFT and mass spectrometry investigation [26]. Furthermore, a theoretical DFT study on the interaction between potassium cation and prolylglycine and

* Corresponding author. Tel.: +32 16327465; fax: +32 16327992.
E-mail address: boeckx@hotmail.com (B. Boeckx).

0301-4622/$ – see front matter © 2011 Elsevier B.V. All rights reserved.
doi:10.1016/j.bpc.2011.07.003

glycylproline has been performed by Abirami et al. [1]. A theoretical MD and DFT study on the conformational behavior of proline and *N*-acetylproline in water have been performed by Aliev et al. [3]. The same others expanded their results with NMR data in different solvents and analyzed also the cis/trans rotameric interconversion [2]. These investigations have not fully explored the position of the carboxylic H which is important with respect to H-bonding.

For a better understanding of the behavior of amino acids in a peptide, matrix-isolation studies supported by theoretical calculations on Ac-L-Pro-NH_2[21], Ac-β-HPro-NHME [8] or Ac-Gly-NHMe and Ac-L-AlaNHMe [20] have been performed with FT-IR and vibration circular dichroisme (VCD) and with IR for Ac-β-HGly-NHMe and Ac-β-HAla-NHMe [5] and the dipeptides of glycine and alanine [11]. In contrast to these studies the aim of this investigation is the behavior of an amino acid as the C-terminus of the peptide. Therefore the only modification of the neutral amino acid is the *N*-acetylation. We have recently demonstrated in a theoretical and FT-IR matrix-isolation study on *N*-acetylcysteine [6] that conformations with or without intramolecular hydrogen bond could be distinguished in an argon matrix and their abundances could be estimated as 97% for the non-H-bonded and 3% for the H-bond bearing conformations. To the best of our knowledge the present study presents the first matrix-isolation IR investigation of NAP.

2. Computational calculations

The conformational landscape of *N*-acetylproline was investigated using successive higher computational methods. In a first stage the total set of 432 NAP structures with varying dihedral angles was optimized at the HF/3-21G level of theory. This cheap and fast computational level reduces the number of interesting conformations. All the forms with a relative energy smaller than 22 kJ.mol^{-1} were further optimized using the density functional theory (DFT), including Becke's nonlocal hybrid three-parameter exchange functional (B3) [4], in combination with the Lee–Yang–Parr (LYP) [16] correlation functional, and afterward with the Møller–Plesset second-order perturbation theory (MP2) [17]. Weak interactions (e.g. dispersion) are known to be poorly described by DFT. However for amino acids, where these interactions are H-bonds, DFT is suitable because H-bonds are principally electrostatic and these are well accounted by DFT or MP2 methods [19]. For both methods the valence double-ζ basis set expanded with diffuse end polarization functions for small as well as large atoms 6-31++G** was used.

The frequencies and the thermodynamical properties of the conformations with low energy were calculated at both the DFT (B3LYP)/6-31++G** and MP2/6-31++G** levels of theory. The harmonic DFT vibrations were scaled with variable scaling factors, i.e. 0.95 for ν(X–H), 0.98 for γ and τ, 0.975 for all other modes, while the ZPE is corrected by 0.97 for the anharmonicity. These factors were optimized for comparison with the matrix-isolation FT-IR spectra of small biomolecules in a former study [29]. The DFT method provides an adequate compromise between the desired chemical accuracy and the computational cost. This method has been successfully applied for studies of amino acids and their derivates [6,9,12,14,15,23].

All calculations were performed using the Gaussian 03 ab initio software package [7] on the high performance computing Linux cluster of the University of Leuven.

The potential energy distributions (PED) were obtained from the force constant matrix and the coordinates of each conformation using a special software package designed for this purpose by Dr. L. Lapinski (Institute of Physics, Pol. Acad. of Sciences, Warsaw, Poland) [25].

The rotamerization constant K_r was calculated using the formula $\Delta G^\circ = -RT \ln K_r$, with ΔG° the difference in Gibbs free energy. From the computed K_r values the theoretical abundances could be estimated.

Theoretical spectra were simulated using the theoretical DFT intensities and frequencies taking into account the relative MP2 abundance of each conformation and using Lorentzian line shapes with 2 cm^{-1} full width at half height.

3. Experimental methods

The FT-IR spectra of NAP isolated in Ar in the range 4000–600 cm^{-1} were obtained by Fourier-transforming 64 interferograms with a Bruker IFS66 spectrophotometer at a resolution of 1 cm^{-1}.

NAP was sublimated in a home-made mini furnace to create a gas mixture with a large excess of Ar. This mixture was deposited onto the CsI window kept at 18 K which was cooled with an closed-cycle helium refrigeration system APD Cryogenics 202 6.5 K [10]. The optimal sublimation temperature to obtain a matrix with monomeric NAP appeared to be 313 K in combination with a $1.5\times10-5$ mbar argon pressure in the cryostat. At this temperature, no decomposition of NAP occurred which was demonstrated by examining the FT-IR spectra of solid NAP before and after heating in the furnace.

N-acetylproline (purity>98%) was obtained from Sigma-Aldrich and was used without further purification. High purity argon gas (99.99990%) was purchased from Air Liquid.

4. Results

The conformational behavior of *N*-acetyl-proline was evaluated by systematic variation of the dihedral angles to create starting structures for geometry optimization (Fig. 1). The chosen values for the $C^{ac}N-C^{\alpha}C^{\beta}$ (a), $C^{\alpha}N-C^{ac}C^{m}$ (d) and $NC^{\alpha}-C^{ca}{=}O$ (b) angles were 0, 60, 120, 180, 240 and 300°, and 0 and 180° for $HO-C^{ca}{=}O$ (c). No variation for the staggered or eclipsed positions of the CH_3 and CH_2 groups was applied because the calculations developed to the most stable geometry independent of the starting structure due to the small difference. This limits the number of possible structures to 432 ($6\times6\times6\times2$) and these were optimized at the HF/32-1G level of theory. This resulted in 10 different conformations with an energy difference smaller than 22 kJ.mol^{-1} relative to the most stable conformation at this level of theory. These obtained minima were used as starting conformations for DFT(B3LYP)/6-31++G** optimizations which yielded six different conformations. Finally these six geometries were subjected to MP2 optimizations.

Table 1 lists the energy and dipole moment data obtained by both the DFT and MP2 methodologies. It appears that the dipole moments

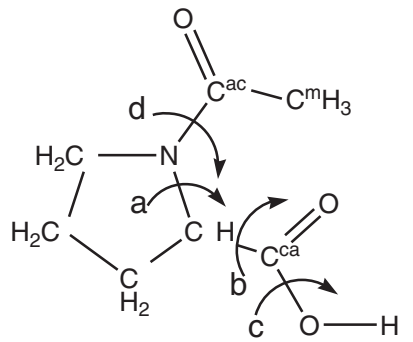

a.6-fold: 0, 60, 120, 180, 240, 300
b.6-fold: 0, 60, 120, 180, 240, 300
c.2-fold: 0, 180
d.6-fold: 0, 60, 120, 180, 240, 300

Fig. 1. The performed variations of the possible internal rotations (deg) in N-cetylproline.

Table 1
DFT(B3LYP)/6-31++G** and MP2/6-31++G** energies, zero-point vibrational energies (ZPE), relative energies (ΔE) and dipole moments (μ) for the most stable N-acetyl-L-proline conformations.

Conformation	Energy (au)	ZPE[a] (au)	Total energy[b] (au)	ΔE[c] (kJ mol^{-1})	μ (D)
DFT					
NAP1	−553.868701	0.176985	−553.691716	0.00	6.90
NAP2	−553.864143	0.176533	−553.687610	10.78	4.33
NAP3	−553.863418	0.176496	−553.686922	12.59	4.46
NAP4	−553.863418	0.176471	−553.686348	14.09	5.55
NAP5	−553.862015	0.176360	−553.685655	15.91	5.10
NAP6	−553.861471	0.176428	−553.685043	17.52	3.03
MP2					
NAP1	−552.279995	0.180753	−552.099243	0.00	7.30
NAP2	−552.277637	0.180171	−552.097466	4.66	4.59
NAP3	−552.276474	0.180145	−552.096330	7.65	4.80
NAP4	−552.276435	0.180096	−552.096339	7.62	6.21
NAP5	−552.275237	0.179748	−552.095490	9.85	5.56
NAP6	−552.274717	0.179862	−552.094854	11.52	2.88

[a] ZPE values scaled with the uniform scaling factor 0.97.
[b] ZPE corrected energies.
[c] Energy difference between the different conformations relative to the most stable conformation NAP1.

and the relative energetic order of the conformations are similar for the DFT and MP2 methodologies. Also the optimized DFT and MP2 geometries are similar as illustrated in Fig. 2.

The most stable conformation at both levels of theory is the conformation NAP1, obviously because of the intramolecular hydrogen bond OH…O═C^{ac}. This conformation is energetically favored by 10.78 and 12.59 kJ.mol^{-1} (DFT) or by 4.66 and 7.65 kJ.mol^{-1} (MP2), with respect to the forms NAP2 and NAP3, respectively.

The energy difference between NAP1 and the other five conformations is much larger than the differences between the latter five, some of these deserve further comment.

The Mulliken atomic charge of the H atom of NAP1 involved in a H-bond is +0.48. This is clearly more positive compared to the other conformations +0.41 for NAP2 and NAP3 and +0.43 for NAP4 and NAP5. Furthermore, the charge of the acetyl O atom in NAP1 is −0.65 which is significantly more negative compared to the charge −0.60 of NAP2–NAP6. This electron redistribution due to the H-bond is also observed in the NBO calculations where electrons of the C–O bond orbitals are delocalized toward unoccupied O═C^{ac} orbitals. In the conformations without H-bond no significant charge delocations toward the acetyl group is observed. These observations confirm the important H-bond interaction in view of the stability of NAP1.

The difference between NAP2 and NAP3 is due to the puckering down (NAP2) and puckering up (NAP3) conformation. Puckering down and puckering up (C$^{\gamma}$-endo and C$^{\gamma}$-exo relative to the COOH group, respectively) conformations are defined by the position of the C$^{\gamma}$ atom and the COOH group which can lie either on the same (puckered down) or on the opposite (puckered up) site of the plane defined by the three atoms N, C$^{\alpha}$ and C$^{\beta}$. Consequently the orientation of the hydrogen atoms of the C$^{\beta}$H$_2$ group is different in NAP2 and NAP3. The existence of both puckered up and down conformations has also been observed in a former study on *N*-acetyl-proline-*N*,*N*-dimethylamide [13].

The difference between NAP4, with a relative energy difference toward NAP1 of 14.09 (DFT) or 7.62 kJ.mol^{-1} (MP2), compared to NAP2 and NAP3 is due to the orientation of the COOH group. The value of the dihedral angle O═C^{ca}–C$^{\alpha}$–N is −27 and −35° in NAP2 and NAP3, which one can call a zusammen geometry, whereas this angle is around 157° in NAP4, i.e. an entgegen geometry (Table 2).

The dihedral angle C$^{\alpha}$N–C^{ac}═O can be used to define the cis and trans conformations of the Ac-Pro peptide bond. In the four most stable structures the dihedral angle C$^{\alpha}$N–C^{ac}═O is small (NAP1) to very small (NAP2–NAP4) (cis) contrary to the conformations NAP5 (ΔE_{DFT} = 15.91 or ΔE_{MP2} = 9.85 kJ.mol^{-1}) and NAP6 (ΔE_{DFT} = 17.52 or ΔE_{MP2} = 11.5 kJ.mol^{-1}) in which this dihedral angle is about 178° (trans) with the acetyl group rotated about the C^{ac}–N bond.

In our former study on *N*-acetyl-cysteine, the cis form has been observed in the most stable conformation and the energy differences with the most stable trans conformation, 9.50 (DFT) or 12.58 (MP2) kJ.mol^{-1}, are of the same order of magnitude as the values of NAP5

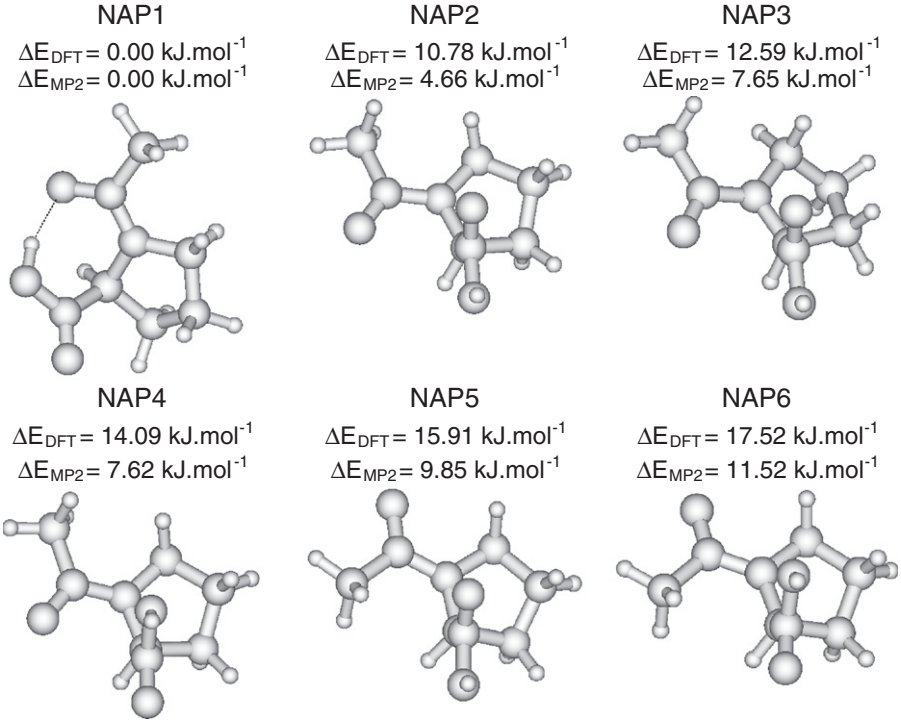

Fig. 2. Optimal geometries (MP2/6-31++G**) and relative energies (MP2/6-31++G** and DFT(B3LYP)/6-31++G**) of the six most stable conformations of N-acetylproline.

Table 2
Geometry parameters of the six most stable conformations of N-acetylproline: distances (Å), angles (deg) and dihedral angles (deg).

	NAP1	NAP2	NAP3	NAP4	NAP5	NAP6
Distances (Å)						
$C^{\alpha}-N$	1.478	1.453	1.456	1.455	1.449	1.450
$N-C^{\delta}$	1.473	1.469	1.462	1.469	1.470	1.470
$C^{\delta}-C^{\gamma}$	1.527	1.531	1.526	1.531	1.529	1.530
$C^{\gamma}-C^{\beta}$	1.530	1.532	1.532	1.531	1.531	1.531
$C^{ac}-N$	1.356	1.368	1.367	1.367	1.369	1.368
$C^{m}-C^{ac}$	1.507	1.510	1.510	1.510	1.514	1.514
$C^{\alpha}-C^{ca}$	1.538	1.520	1.517	1.520	1.522	1.523
$C^{ca}=O$	1.221	1.220	1.219	1.219	1.219	1.221
$C^{ac}=O$	1.254	1.241	1.241	1.241	1.239	1.240
$C^{ca}-O$	1.344	1.358	1.357	1.363	1.363	1.359
$C^{m}-H$	1.090	1.092	1.091	1.086	1.086	1.086
$C^{m}-H$	1.086	1.090	1.086	1.092	1.091	1.091
$C^{m}-H$	1.091	1.086	1.091	1.090	1.091	1.091
O–H	0.990	0.973	0.973	0.974	0.974	0.975
$C^{\beta}-H$	1.087	1.090	1.092	1.090	1.090	1.090
$C^{\gamma}-H$	1.090	1.090	1.092	1.090	1.090	1.090
$C^{\delta}-H$	1.090	1.090	1.096	1.090	1.090	1.090
$C^{\delta}-H$	1.095	1.095	1.089	1.095	1.093	1.093
$C^{\gamma}-H$	1.091	1.090	1.090	1.090	1.091	1.091
$C^{\beta}-H$	1.092	1.092	1.089	1.092	1.092	1.092
$C^{\alpha}-H$	1.094	1.090	1.092	1.090	1.092	1.091
O…H[a]	1.733					
Angles (deg)						
$C^{\alpha}-N-C^{\delta}$	112.1	113.1	112.7	113.3	113.1	113.1
$N-C^{\delta}-C\gamma$	102.7	103.0	101.6	103.0	103.1	103.2
$C^{\delta}-C^{\gamma}-C^{\beta}$	103.0	103.4	102.6	103.3	103.6	103.7
$C^{ac}-N-C^{\delta}$	125.8	126.9	128.0	127.0	120.3	120.4
$C^{m}-C^{ac}-N$	117.4	116.7	116.7	116.6	116.7	116.6
$C^{ca}-C^{\alpha}-N$	110.7	110.2	110.4	112.9	112.0	114.5
$O=C^{ca}-C^{\alpha}$	123.0	125.2	124.7	124.0	126.0	123.5
$O=C^{ac}-N$	121.0	120.6	120.3	120.6	120.9	120.9
$C^{ca}-C^{\alpha}-N$	114.9	111.0	111.2	112.6	110.4	112.9
$C^{ac}-C^{m}-H$	111.6	109.7	110.9	108.1	107.8	107.8
$C^{ac}-C^{m}-H$	108.0	112.0	108.0	109.8	111.4	111.0
$C^{ac}-C^{m}-H$	110.1	108.1	110.8	112.0	110.9	111.5
$C^{ca}-O-H$	109.3	106.6	106.5	105.8	106.7	106.2
$C\gamma-C^{\beta}-H$	113.2	113.6	109.6	113.8	114.2	114.3
$C\delta-C^{\gamma}-H$	111.9	112.2	109.5	112.2	112.4	112.3
$N-C^{\delta}-H$	110.6	110.9	111.1	110.9	109.8	109.9
$N-C^{\delta}-H$	110.3	110.4	110.8	110.5	109.7	109.6
$C\delta-C^{\gamma}-H$	110.2	109.6	112.8	109.7	110.0	110.1
$C\gamma-C^{\beta}-H$	110.4	110.7	113.7	110.5	110.6	110.5
$N-C^{\alpha}-H$	108.7	111.2	110.7	111.1	112.3	112.2
Dihedral angles (deg)						
$C^{\gamma}-C^{\delta}-N-C^{\alpha}$	−14.1	−8.4	26.0	−9.8	−5.9	−4.7
$C^{\beta}-C^{\gamma}-C^{\delta}-N$	33.3	29.0	−37.9	29.5	27.8	26.7
$C^{ac}-N-C^{\delta}-C^{\gamma}$	177.2	156.7	−163.3	158.3	168.2	170.7
$C^{m}-C^{ac}-N-C^{\delta}$	−3.0	9.8	5.2	8.4	−176.3	177.8
$C^{ca}-C^{\alpha}-N-C^{\delta}$	109.7	102.7	115.6	106.4	99.8	100.1
$O=C^{ca}-C^{\alpha}-N$	−117.7	−27.3	−35.0	157.4	−15.1	165.7
$O=C^{ac}-N-C^{\alpha}$	10.1	−1.0	−1.1	−0.9	−178.0	−178.0
$O-C^{ca}-C^{\alpha}-N$	63.1	156.5	149.6	−26.7	166.7	−16.3
$N-C^{ac}-C^{m}-H$	50.8	−76.8	63.6	165.7	−178.1	177.6
$N-C^{ac}-C^{m}-H$	171.7	43.6	−176.7	−75.7	−58.4	−63.0
$N-C^{ac}-C^{m}-H$	−69.3	164.7	−56.7	44.6	62.6	57.8
$O=C^{ca}-O-H$	177.8	1.5	2.3	−3.3	−1.1	0.0
$C^{\delta}-C^{\alpha}-C^{\beta}-H$	−161.2	−160.5	−79.9	−160.4	−160.7	−160.2
$N-C^{\delta}-C^{\gamma}-H$	155.3	151.1	79.4	151.5	149.5	148.5
$C^{\alpha}-N-C^{\delta}-H$	−135.2	−128.7	−92.4	−130.2	−127.3	−126.1
$C^{\alpha}-N-C^{\delta}-H$	104.4	110.8	146.4	109.3	114.1	115.4
$N-C^{\delta}-C^{\gamma}-H$	−83.7	−88.3	−159.5	−87.9	−89.8	−91.0
$C^{\delta}-C^{\gamma}-C^{\beta}-H$	75.9	77.3	158.7	77.5	76.4	76.9
$C^{\delta}-N-C^{\alpha}-H$	−131.5	−137.0	−123.8	−134.7	−138.1	−138.6

[a] The distance of the intramolecular H-bond OH…O=C^{ac} in NAP1.

($\Delta E_{DFT} = 15.91$ or $\Delta E_{MP2} = 9.85$ kJ.mol^{-1}) observed here. Finally, the difference between NAP5 and NAP6 is due to the orientation of the COOH group which is zusammen in NAP5 and entgegen in NAP6.

Close examination of the bond distances reveals the double bond character of the amide bond due to the resonance. The $C^{ac}-N$ distance is clearly intermediate between the typical distances for C–N single and double bonds, i.e. 1.45 and 1.25 Å, respectively. The double bond character is enhanced due to the formation of an intramolecular H-bond in NAP1 since the $C^{ac}-N$ distance (1.356 Å) becomes smaller in these H-bond containing conformation compared to the non-H-bond containing conformation NAP2–NAP6 (1.367–1.369 Å). Due to the formation of the $C^{ca}-O-H\ldots O-C^{ac}$ H-bond, the distances $C^{ac}-O$ and

Table 3
DFT(B3LYP)/6-31++G** and MP2/6-31++G** computed thermodynamical data for N-acetyl-proline at 298.15 K and 313.00 K: relative zero-point corrected energies (ΔE/kJ.mol^{-1}), formation enthalpies (ΔH°/kJ.mol^{-1}), entropy contributions (TΔS°/kJ.mol^{-1}), Gibbs free energies (ΔG°/kJ.mol^{-1}), rotamerization constants (K_r) and abundances (%) for the six most stable conformations.

Conformation	ΔE[a]	ΔH°	TΔS°	ΔG°	K_r	%[b]	ΔH°	TΔS°	ΔG°	K_r	%
DFT											
		298.15 K[c]					313.00 K[d]				
NAP1	0.0	0.00	0.00	0.00	1.00	91.23	0.00	0.00	0.00	1.00	88.93
NAP2	10.78	12.06	4.27	7.79	0.04	3.94	12.12	4.54	7.58	0.05	4.84
NAP3	12.59	13.96	4.71	9.25	0.02	2.19	14.03	5.01	9.01	0.03	2.76
NAP4	14.09	15.42	4.74	10.68	0.01	1.23	15.48	5.03	10.44	0.02	1.61
NAP5	15.91	17.37	5.85	11.52	<0.01	0.87	17.43	6.21	11.22	0.01	1.19
NAP6	17.52	18.99	5.96	13.13	<0.01	0.54	19.05	6.21	12.84	<0.01	0.64
MP2											
		298.15 K[c]					313.00 K[d]				
NAP1	0.00	0.00	0.00	0.00	1.00	51.60	0.00	0.00	0.00	1.00	47.66
NAP2	4.66	5.84	3.76	2.07	0.43	22.39	5.89	4.01	1.88	0.48	23.12
NAP3	7.65	8.93	4.41	4.53	0.16	8.30	8.99	4.68	4.31	0.19	9.11
NAP4	7.62	8.81	3.89	4.92	0.14	7.09	8.87	4.14	4.73	0.16	7.78
NAP5	9.85	11.49	6.65	4.84	0.14	7.29	11.55	7.04	4.51	0.18	8.42
NAP6	11.52	13.01	6.20	6.82	0.06	3.30	13.07	6.57	6.51	0.08	3.91

[a] ZPE corrected energy relative to NAP1: $E_{DFT} = -553.691716$ a.u. and $E_{MP2} = -552.099243$ a.u.
[b] Only taking into account the six most stable conformations.
[c] Relative to NAP1. Absolute values for NAP1 at 298.15 K: $H°_{DFT} = -553.676856$ a.u., $H°_{MP2} = -552.087932$; $TS°_{DFT} = 0.047703$ a.u., $TS°_{MP2} = 0.047414$ a.u.; $G°_{DFT} = -553.727987$ a.u., $G°_{MP2} = -552.135346$ a.u.
[d] Relative to NAP1. Absolute values for NAP1 at 313 K: $H°_{DFT} = -553.679295$ a.u., $H°_{MP2} = -552.086957$; $TS°_{DFT} = 0.051091$ a.u., $TS°_{MP2} = 0.050774$ a.u.; $G°_{DFT} = -553.730387$ a.u., $G°_{MP2} = -552.137731$.

O–H are typically elongated in NAP1 in contrast to the reduced distance C^{ca}–O.

All the geometric properties of the six most stable conformations are summarized in Table 2 and the coordinates are found in the supplementary information.

Table 3 lists the theoretically calculated thermodynamical properties including the abundances of the most stable conformations of NAP at both room temperature and the sublimation temperature applied for NAP in argon (313.00 K). The relative order of the Gibbs free energies is in line with that of the electronic energies, except for NAP5 at the MP2/6-31++G** level where ΔG becomes negligibly smaller than for NAP4.

The MP2 entropy term TΔS° at sublimation temperature is 4.01 kJ.mol^{-1} smaller for NAP1 than for NAP2. Such a smaller entropy contribution to the stability is characteristic for H-bonded conformations. The value obtained here is comparable with that obtained for other amino acids, e.g. 2.9 kJ.mol^{-1} for alanine [14], 7.2 kJ.mol^{-1} for glycine [24] and 7.74 kJ.mol^{-1} for *N*-acetyl-cysteine [6].

The theoretical rotamerization constant for the different conformational equilibria can be calculated using the equation $\Delta G° = \Delta H° - T\Delta S° = -RT \ln K_r$ which allows to predict the abundances of the different conformations in the matrix. It should be mentioned here that for this estimation, we have only taken into account the six most stable conformations of NAP. At the applied sublimation temperature of 313 K, NAP1 is clearly the most dominant conformation in the matrix with an abundance of 89% (DFT) or 48% (MP2). Considering the MP2 abundances of NAP2, NAP3, NAP4 and NAP5, which are all larger than 5%, these conformations are also expected to be present in the matrix in trace amounts.

NAP1 is the only conformation with an intramolecular H-bond and for this reason the vibrational modes involved in the H-bond (ν(OH), δ(OH), γ(OH), ν(C═O), δ(C═O) and γ(C═O)) can be easily used to distinguish this conformation from the others. At the contrary, since the difference in geometry between NAP2 up to NAP6 is mainly due to the rotation of the $C{=}O^{ac}$ and COOH groups, the calculated values of the most intense IR absorptions barely differ, as presented in Table 4. Since it is extremely difficult to distinguish between these forms in the matrix, we have grouped together the spectral assignments for NAP2 up to NAP6. Furthermore, since many bands of this group will overlap with those of the dominant conformation NAP1, only the relevant bands of NAP2–NAP6 are mentioned further.

Fig. 3 presents (a) the theoretical spectrum with the scaled DFT frequencies and taking into account the MP2 abundances at the sublimation temperature and (b) the overall (4000–600 cm^{-1}) experimental FT-IR spectrum in Ar at the sublimation temperature 313 K. FT-IR spectra of NAP in a KBr pellet scanned before and after

Table 4
The most intense theoretically predicted (scaled)[a] modes of the non-H-bonded conformations NAP2–NAP6.

PED[b]	NAP2		NAP3		NAP4		NAP5		NAP6	
	$\bar{\nu}$ (cm^{-1})	I (km.mol^{-1})	$\bar{\nu}$ (cm^{-1})	I (km.mol^{-1})	$\bar{\nu}$ (cm^{-1})	I (km.mol^{-1})	$\bar{\nu}$ (cm^{-1})	I (km.mol^{-1})	$\bar{\nu}$ (cm^{-1})	I (km.mol^{-1})
ν (O–H)	3566	71	3567	74	3566	71	3564	73	3561	76
$\nu\ (C{=}O)^{ca}$	1775	244	1778	256	1771	349	1779	256	1764	313
$\nu\ (C{=}O)^{ac}$	1683	352	1684	341	1684	331	1687	385	1685	409
ν (C–O) + δ (OH)	1124	332	1128	330	1143	98	1113	323	1138	116
$\nu\ (N-C^{ac})$	1399	326	1406	326	1401	345	1397	327	1394	331
γ (OH)	581	77	638	59	638	59	603	78	611	66
$\delta(C^{\alpha}-C^{ca}) + \nu\ (C^{\alpha}-C^{\beta})$	732	27	727	34	726	25	723	30	734	28

[a] Variable scaling factors used for DFT: 0.95 for ν (X–H); 0.98 for γ and τ; 0.975 for all other modes.
[b] Only most important PED contribution.

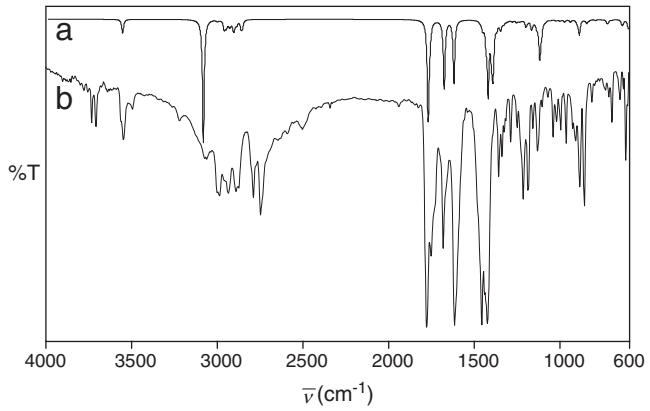

Fig. 3. Theoretical (a) and experimental (b) IR spectra of N-acetylproline in Ar at 18 K.

heating in the furnace showed that no decomposition of the compound occurred during heating. The experimental spectrum is almost water-free (3700–3500 cm^{-1} and 1650–1580 cm^{-1}) which is important because we are focusing on the assignments of possible H-bond acceptors and donors. A survey of the theoretical DFT and experimental frequencies, intensities and PEDs of NAP1 is presented in Table 5.

In the high frequency region (Fig. 4) the important mode ν(OH) is located. In the experimental spectrum this region is clearly dominated by the very broad and intense band extending from ±3400 to 2400 cm^{-1}. This band can be assigned to the H-bonded mode ν(OH…) of the most dominant conformation NAP1. The center of this band is located at about 2900 cm^{-1} while it is theoretically predicted at 3093 cm^{-1}. The former experimental value is considerably smaller than the observed ν(OH…) frequency for proline [28] (3025 cm^{-1}). This larger red shift in NAP can be explained by the stronger intramolecular H-bond OH…O═C^{ac} in NAP compared to the H-bond N…HO in proline which is clearly demonstrated by the smaller distance (MP2) O…H in NAP1 (1.733 A) compared to the distance N…H in proline (1.827 Å) (Table 2).

Two other bands observed in the ν(OH) region at 3561 and 3547 cm^{-1} are due to the non-H-bonded conformations. The frequency difference with ν(OH…) of NAP1 is as large as ±600 cm^{-1}. The theoretical values for ν(OH) of NAP2–NAP6 are too close to each other (3561–3567 cm^{-1}) to assign these bands to a specific conformation.

Two relatively weak bands are observed at 3495 and 3220 cm^{-1}, while no theoretical bands are predicted near these values. The most probable origin of these bands are overtones of the ν(C═O…) bands at 1753 and 1616 cm^{-1}, respectively. All the C–H stretching modes, predicted between 3014 and 2873 cm^{-1} are superimposed on the broad ν(OH…) absorption of NAP1. Due to the small intensity of these bands, the ν(CH) modes can only be tentatively assigned to the bands in the region between 3037 and 2874 cm^{-1}. Rather surprisingly we observe 2 additional bands shifted down about 100 cm^{-1} below the predicted ν(CH) vibrations, at 2789 and 2746 cm^{-1}, respectively. In the FT-IR spectrum of pure NAP in a KBr pellet, we also observed these bands below the ν(CH) region. Therefore we can exclude that these bands are due to reduction of the compound NAP to an aldehyde during deposition of the matrix. In a previous study of proline [28] these bands were not observed in the matrix and therefore these bands must originate from the additional acetyl group of the studied compound. The band at 2789 cm^{-1} might be a combination band of the intense band at 1616 cm^{-1} and the band at 1188 cm^{-1}, both being assigned to NAP1, the first being due to ν(C═O) of the acetyl group. The other band at 2746 cm^{-1} might be a combination band of the intense bands observed at 1682 and 1071 cm^{-1}. The band at 1682 cm^{-1} is due to ν(C═O)^{ac} of the non-H-bonded group whereas the band at 1071 cm^{-1} is an overlap of bands of the conformations NAP1 till NAP6 and partly due to the acetyl group (ρ^1(CH$_3$), ρ^2(CH$_3$) and ν (C^{ac}–C^{m}) in NAP2–NAP6).

In the region 2000–600 cm^{-1} (Fig. 5) the very intense IR absorption of the mode ν(C═O) is located. The most intense band at 1779 cm^{-1} is a superposition of the ν (C═O)^{ca} modes of conformations NAP1 till NAP6. The two reasons for this are that the predicted values do not significantly differ (1779–1764 cm^{-1}) and ν(C═O)^{ca} is predicted as an intense absorption. The weaker band observed at 1753 cm^{-1} with a low-frequency shoulder is probably due to self-aggregation of NAP. This assignment is supported by the fact that this band has a larger intensity in a separate matrix-isolation FT-IR spectrum of NAP taken at a higher sublimation temperature, which is available as supplementary information. The observation that the intensity of the band at 3495 cm^{-1} is also larger in this separate experiment confirms the assignment to an overtone of the band at 1753 cm^{-1}.

The ν(C═O) mode of the acetyl group is an extremely important vibration to be analyzed because this C═O group is involved in the H-bond in NAP1, which permits to distinguish between NAP1 and the non-H-bonded conformations. Two bands are observed i.e. at 1682 and at 1616 cm^{-1} (very intense). The first one can be assigned to the ν(C═O)^{ac} modes of the non-H-bonded group predicted between 1683 and 1687 cm^{-1}, whereas the somewhat broadened band at 1616 cm^{-1} must be due to the H-bond involving the (C═O)^{ac} group with a predicted value of 1627 cm^{-1}. The presence of these two bands in the experimental spectrum is a second evidence for the simultaneous existence of the H-bonded (NAP1) as well as the non-H-bonded conformations in the matrix.

The δ(OH) and γ(OH) modes are two other important spectral tools for evaluating H-bonding. The δ(OH…) mode of NAP1 has a significant PED contribution to the predicted bands at 1427 and 1409 cm^{-1}. In the experimental spectrum two intense bands are observed at 1456 and 1424 cm^{-1}. The band at 1456 cm^{-1} is assigned to the δ(OH…) mode of NAP1 since the δ(N–C^{ac}) of NAP2–NAP6 is predicted as an intense mode at 1406–1394 cm^{-1} which matches the experimental band at 1424 cm^{-1}.

For the non-H-bonded NAP conformations, the PED distribution for the δ(OH) mode indicates strong coupling with other modes. The bands predicted between 1143 and 1113 cm^{-1} have PED contributions of both ν(C–O) and δ(OH). In the experimental spectrum we observe a band at 1132 with a shoulder at 1125 cm^{-1} which cannot, in comparison with the theoretical calculations, be assigned to NAP1. For this reason, and because ν(C–O) + δ(OH) is predicted to be very intense, the band at 1132 cm^{-1} must be due to the non-H-bonded conformations. The fact that there is a shoulder at 1125 cm^{-1} again demonstrates that there are at least two non-H-bonded conformations present in the matrix. These experimental frequency values of the δ(OH) mode imply a positive frequency shift of about 300 cm^{-1} for the H-bonded δ(OH…) mode of NAP1. This is rather high for a δ(OH…) mode, but not unexpected in view of the large $\Delta\nu$(OH…) shift mentioned earlier.

In the γ(OH) region a slightly broadened band is observed at 890 cm^{-1}. This band can be assigned to the H-bonded γ(OH…) mode of NAP1 in view of the calculated value of 893 cm^{-1}. The predicted γ(OH) frequencies of the non-H-bonded conformations vary from 638 to 581 cm^{-1}. In the spectrum, candidate bands are observed at 650, 631, 616 and 606 cm^{-1}. Predicted frequency values in this region for the most abundant conformation NAP1 are 635, 607 and 596 cm^{-1}, which explains the presence of the latter 3 observed bands. Probably the band at 650 cm^{-1} can be assigned to the γ(OH) mode of the non-H-bonded conformations predicted at 638 cm^{-1} for both the conformations NAP3 and NAP4. This assignment suggests that at least one of the forms NAP3 and NAP4 is present in the matrix, suggesting a positive experimental frequency shift of 240 cm^{-1} for γ(OH…) of NAP1.

At 734 and 716 cm^{-1} two relatively weak bands are observed, although no theoretical bands are predicted here for NAP1. Considering the theoretical frequencies for NAP2–NAP6, these bands can be

Table 5
Experimentally observed frequencies and intensities and theoretical IR spectral data (DFT(B3LYP)/6-31++G**) for the most abundant conformation (NAP1) of N-acetylproline and other important assignments.

Experimental		Theoretical[a]		
		NAP1		PED[b]
Obsd. $\bar{\nu}$ (cm^{-1})[c]	I[d]	Calc. $\bar{\nu}$ (cm^{-1})	$I_{calc.}$ ($km.mol^{-1}$)	
3561	sh	(See Table 4)		ν (OH) of non-H-bonded NAP[e]
3547	m	(See Table 4)		ν (OH) of non-H-bonded NAP[e]
3495	w	(See text)		Overtone of ν (C═O…) at 1753 cm^{-1}
3220	w	(See text)		Overtone of ν $(C{=}O)^{ac}$ at 1616 cm^{-1}
±2900	vs	3093	326	ν (OH…) (100)
3037	vw	3014	1	ν^{d1} (CH_3) (100)
3000	w	2994	1	ν^{as} ($C^{\beta}H_2$) (90)
2986	w	2970	12	ν^{as} ($C^{\gamma}H_2$) (83)
2961	vw	2959	4	ν^{d2} (CH_3) (99)
2935	w	2941	11	ν^{as} ($C^{\delta}H_2$) (84)
2926	sh	2920	8	ν^{s} ($C^{\gamma}H_2$) (63)
[f]		2914	11	ν (CH) (45) + ν^{s} ($C^{\beta}H_2$) (43)
[f]		2903	4	ν (CH) (53) + ν^{s} ($C^{\beta}H_2$) (41)
2889	m	2899	2	ν^{s} (CH_3) (100)
2874	w	2873	20	ν^{s} ($C^{\delta}H_2$) (87)
2789	m	(See text)		Combination band of 1616 and 1188 cm^{-1}
2746	m	(See text)		Combination band of 1682 and 1071 cm^{-1}
1779	vs	1779	174	ν $(C{=}O)^{ca}$ (84) + ν $(C{=}O)^{ca}$ of non-H-bonded NAP[e]
1753	s			Self-aggregation of NAP[g]
1682	s	(See Table 4)		ν $(C{=}O)^{ac}$ of non H-bonded NAP[e]
1616	vs	1627	168	ν $(C{=}O\ldots)^{ac}$ (75)
1497	sh	1495	0	δ ($C^{\delta}H_2$) (67) + δ ($C^{\gamma}H_2$) (31)
		1474	2	δ ($C^{\gamma}H_2$) (84)
1470	sh	1460	15	δ^{d1} (CH_3) (65) + δ ($C^{\gamma}H_2$) (16) + δ^{d2} (CH_3) (16)
1456	vs	1456	2	δ ($C^{\gamma}H_2$) (54) + δ ($C^{\beta}H_2$) (54) + δ^{1} (ring) (10)
1441	s	1439	42	δ^{d2} (CH_3) (52) + ν (NC_{ac}) (17)
1424	vs	1427	186	δ (OH…) (25) + δ^{d2} (CH_3) (19) + δ^{d1} (CH_3) (19) + ν (NC_{ac}) (16)
1413	sh	1409	47	δ (OH…) (45) + ν (NC) (19)
1359	m	1362	6	δ^{s} (CH_3) (87)
1338	m	1339	1	δ ($C^{\gamma}H_2$) (69) + γ (CH) (11) + δ ($C^{\delta}H_2$) (11)
1326	vw	1334	3	δ ($C^{\delta}H_2$) (62) + δ ($C^{\beta}H_2$) (26) + γ (CH) (12)
1316	vw	1319	1	δ ($C^{\gamma}H_2$) (85)
		1309	2	τ ($C^{\gamma}H_2$) (38) + δ ($C^{\beta}H_2$) (30) + ν ($C^{\beta}C^{\alpha}$) (20)
1287	m	1285	3	δ ($C^{\gamma}H_2$) (82)
1251	w	1245	3	ρ ($C^{\gamma}H_2$) (41) + τ ($C^{\delta}H_2$) (24) + τ ($C^{\beta}H_2$) (15) + γ (ring) (15)
1215	m	1207	13	τ ($C^{\gamma}H_2$) (79) + ν (C–O) (15)
1188	m	1175	10	τ ($C^{\gamma}H_2$) (52) + δ^{d2} (ring) (16) + ν (C–O) (11) + τ ($C^{\beta}H_2$) (10)
1183	m	1172	11	τ ($C^{\gamma}H_2$) (59) + δ^{d2} (ring) (19) + δ^{d1} (ring) (14)
1158	w	1145	5	τ ($C^{\gamma}H_2$) (67) + ν (NC^{α}) (17)
1132	m	(See Table 4)		ν (C–O) + δ (OH) of non-H-bonded NAP[e]
1125	sh	(See Table 4)		ν (C–O) + δ (OH) of non-H-bonded NAP[e]
1104	vw	1098	1	ρ ($C^{\gamma}H_2$) (57) + γ (ring) (19)
1071	vw	1064	0	ρ ($C^{\gamma}H_2$) (58) + δ^{d2} (ring) (14) + γ (ring) (12)
1040	w	1030	2	ρ^{1} (CH_3) (40) + ρ^{2} (CH_3) (30) + γ (CC^{m}) (16)
1023	w	1023	1	δ ($C^{\gamma}H_2$) (53) + ρ^{1} (CH_3) (15)
996	w	981	3	δ ($C^{\gamma}H_2$) (78) + γ (ring) (12) + ν ($C^{\beta}C^{\alpha}$) (11)
964	m	947	6	ν ($C^{\beta}C^{\alpha}$) (25) + ν ($Ca^{c}C^{m}$) (15) + ρ^{2} (CH_3) (15) + δ^{d2} (ring) (14) + ν (NC^{α}) (12) + γ (ring) (11)
926	vw	909	4	ν ($C^{\delta}C^{\gamma}$) (30) + ρ ($C^{\gamma}H_2$) (29) + ν ($C^{\gamma}C^{\beta}$) (13)
909	w	903	6	ρ ($C^{\gamma}H_2$) (75) + ν ($C^{\delta}C^{\gamma}$) (12)
890	m	893	37	γ (OH…) (66) + ν ($C^{\gamma}C^{\beta}$) (24) + τ ($C^{\gamma}H_2$) (11)
		861	0	ρ ($C^{\gamma}H_2$) (58) + δ^{d2} (ring) (21) + δ^{d1} (ring) (11)
858	m	850	9	δ^{d1} (ring) (21) + γ $(C{=}O)^{ca}$ (20) + γ (OH…) (14) + ν (NC^{δ}) (13)
814	w	800	2	ν (C^{α}–C^{ca}) (32) + ρ ($C^{\beta}H_2$) (22) + ρ ($C^{\delta}H_2$) (13) + ρ ($C^{\delta}H_2$) (12) + δ^{d1} (ring) (12) + ν ($C^{\gamma}C^{\beta}$) (11)
734		(See Table 4)		δ (C^{α}–C^{ca}) + ν (C^{α}–C^{δ}) of non-H-bonded NAP2-NAP6[e]
716				
696	w	703	2	ρ ($C^{\gamma}H_2$) (33) + δ $(C{=}O\ldots)^{ac}$ (17) + ν (NC^{δ}) (16) + δ^{d1} (ring) (16) + ν (NC^{α}) (10)
631	w	635	2	ρ ($C^{\gamma}H_2$) (89) + ν ($C^{\beta}C^{\alpha}$) (11)
616	m	607	10	ρ ($C^{\gamma}H_2$) (90)
606	sh	596	3	ρ ($C^{\gamma}H_2$) (60) + γ ($C^{ac}C^{m}$) (27) + γ $(C{=}O\ldots)^{ac}$ (15)
[h]		559	0	ρ ($C^{\gamma}H_2$) (41) + δ $(C{=}O)^{ca}$ (28) + ρ ($C^{\beta}H_2$) (11) + δ (C–O) (10)
[h]		497	4	δ ($C^{\gamma}H_2$) (53) + δ^{d1} (ring) (19) + γ (ring) (13) + δ $(C{=}O\ldots)^{ac}$ (11)
[h]		461	7	ρ ($C^{\gamma}H_2$) (53) + δ(C–O) (34) + δ ($NC^{ac}C^{m}$) (11)
[h]		354	1	δ($NC^{ac}C^{m}$) (29) + δ^{d1} (ring) (27) + δ (C–O) (14)
[h]		319	2	γ (ring) (52) + δ $(C{=}O)^{ca}$ (17) + ρ ($C^{\beta}H_2$) (14) + ρ ($C^{\gamma}H_2$) (12)
[h]		288	6	δ ($NC^{\alpha}C^{ca}$) (58) + δ (C–O) (11)
[h]		230	4	δ ($C^{\delta}NC^{ac}$) (65) + δ (C–O) (23)
[h]		214	4	γ (ring) (59) + γ $(C{=}O\ldots)^{ac}$ (19)
[h]		150	1	γ (ring) (28) + γ (N–C^{ca}) (24) + ρ($C^{\gamma}H_2$) (20) + γ $(C{=}O\ldots)^{ac}$ (17) + γ ($C^{\alpha}C^{ca}$) (12)
[h]		124	1	γ ($C^{ac}C^{m}$) (26) + τ (CH_3) (24) + γ (C–O) (17) + γ (NC^{ac}) – (17) + γ $(C{=}O\ldots)^{ac}$ (13)
[h]		104	1	γ (CC^{ca}) (35) + τ (CH_3) (33) + γ (NC^{ac}) (21) + γ ($C^{ac}C^{m}$) (12)

(continued on next page)

Table 5 (*continued*)

Experimental		Theoretical[a]		
		NAP1		PED[b]
Obsd. $\bar{\nu}$ (cm^{-1})[c]	I[d]	Calc. $\bar{\nu}$ (cm^{-1})	$I_{calc.}$ ($km.mol^{-1}$)	
[h]		93	1	γ ($C^{\alpha}C^{ca}$) (39) + τ (CH_3) (36) + γ (C–O) (16) + γ (ring) (10)
[h]		74	2	γ (C═O…)^{ca} (39) + γ (C–O) (27) + δ ($C^{ca}C^{\alpha}N$) (12)

[a] Variable scaling factors: 0.95 for ν (X–H); 0.98 for γ and τ; 0.975 for all other modes.
[b] Potential energy distribution (%); only contributions >10% are listed; subscripts ac and ca denote acetyl and carboxylic acid, respectively.
[c] Observed frequency in the matrix FT-IR spectrum of N-acetylproline.
[d] Relative experimental intensity denoted as vs (very strong), s (strong), m (medium), w (weak), vw (very weak) and sh (shoulder).
[e] Observed mode of non-H-bonded NAP (NAP2–NAP6).
[f] Not observed in the spectrum.
[g] This ν(C═O…) band is due to self-aggregation of NAP.
[h] Situated below the studied region 4000–600 cm^{-1}.

assigned to $\delta(C^{\alpha}-C^{ca})+\nu(C^{\alpha}-C^{\beta})$ of NAP2–NAP6 with predicted values between 723 and 734 cm^{-1}, respectively.

In the spectrum obtained at a higher sublimation temperature (not shown) the bands assigned to the vibrations of the free OH modes of the non-H-bonded conformations 3561 and 3546 cm^{-1} ν(OH), 1132 and 1125 cm^{-1} δ(OH) and 850 cm^{-1} γ(OH) are shifted or have completely disappeared. This is an additional proof for the proposed assignments to the OH group, capable of H-bonding.

Due to overlap of many bands of the abundant NAP1 conformation, it is not possible to estimate each rotamerization constant between the separate conformations (K_r(NAP1/NAP2), K_r(NAP1/NAP3),…). However a global rotamerization constant K_r between the form NAP1 and the non-H-bonded forms (NAP2–NAP6) can be estimated:

$$K_r = \frac{[(NAP2-NAP6)]}{[NAP1]} = \frac{\left(I_{exp}/I_{theor}\right)_{(NAP2-NAP6)}}{\left(I_{exp}/I_{theor}\right)_{NAP1}},$$

with I_{exp} and I_{theor} the experimental and theoretical calculated intensities of characteristic IR absorption bands (Table 6). The theoretical group intensity of (NAP2–NAP6) can be obtained from the theoretically predicted abundances of these conformations. The experimental ν(OH) bands at 3561 and 3546 cm^{-1} are perfectly suitable for (NAP2–NAP6) because these bands are located in an area where no other overlapping bands are present. On the other hand, the ν (C═O)^{ac} at 1616 cm^{-1} of NAP1 has no or little contribution of (NAP2–NAP6) and is therefore also a suitable band to be used. Combining these intensity measurements for (NAP2–NAP6) and NAP1, this results in a rotamerization constant for NAP1 (NAP2–NAP6) of 0.50. From this value the abundances can be derived. It appears that NAP1 is abundant for 67% and (NAP2–NAP6) for 33%, whereas the predicted K_r (MP2) values at the sublimation temperature are 48% (NAP1) and 52% (NAP2–NAP6). The observed difference can be explained by the fact that the used vibration ν(C═O)^{ac} of NAP1 is a broadened band due to the H-bond and therefore it is difficult to integrate. Consequently the results of this rough estimation must be carefully interpreted.

The mean frequency deviation of all the assigned modes of NAP1, $\sum|\bar{\nu}_{theor}-\bar{\nu}_{exp}|/n$, with n the number of the assigned modes, is 12.4 cm^{-1} (all modes) or 7.8 cm^{-1}, when not taking into account the ν(OH) mode with a considerably larger deviation due to H-bonding. A frequency inaccuracy of about 10 cm^{-1} is of the order of magnitude formerly observed for amino acids when variable scaling factors are used [22].

5. Conclusions

To investigate the conformational landscape of N-acetylproline, optimizations at the successive HF/3-21G, DFT(B3LYP)/6-31++G** and MP2/6-31++G** levels of theory were performed. This resulted in six stable MP2 conformations with a relative energy difference smaller than 12 $kJ.mol^{-1}$. Among these, the conformation NAP1 with an intramolecular H-bond appeared to be significantly more stable than NAP2–NAP6. The entropy $T\Delta S°$ term for NAP1 is 3.8 to 4.5 $kJ.mol^{-1}$ smaller compared to NAP2, which is a typical value compared to other amino acids [14,23] or derivatives [6]. The theoretical rotamerization constant and the abundances could be derived from the $\Delta G°$ value. NAP1 (47%) is clearly the most abundant conformation, but NAP2 (23%), NAP3 (9%) NAP4 (8%) and NAP5 (8%) are also expected to be present in the low temperature matrix.

In the experimental matrix-isolation FT-IR spectrum, NAP1 is dominantly present and can be easily distinguished from the non-H-bonded conformations by the H-bonded modes ν(OH…), ν(C═O…)^{ac}

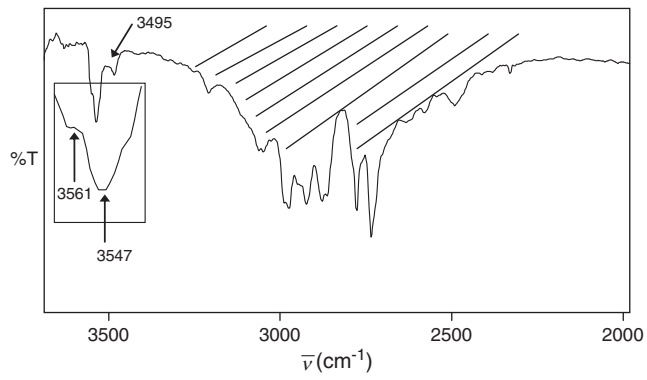

Fig. 4. The high frequency region of the experimental FT-IR spectrum of N-acetylproline in Ar at 18 K.

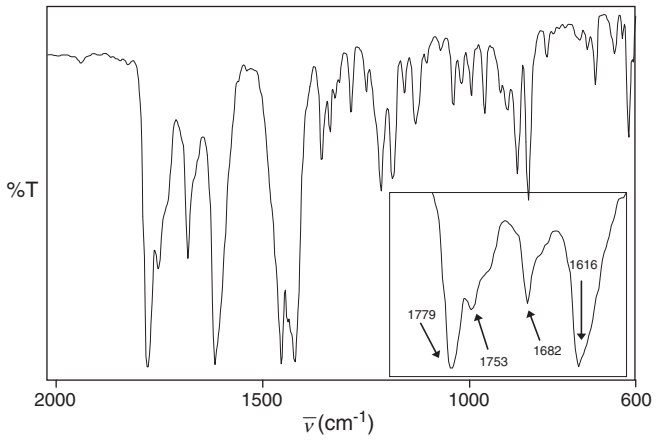

Fig. 5. The low-frequency region (2000–600 cm^{-1}) of the experimental matrix-isolation FT-IR spectrum of N-acetylproline in argon at 18 K.

Table 6
DFT(B3LYP)/6-31++G** frequencies and intensities of ν(C═O…)^{ac} and ν(OH) modes in different conformations of N-acetylproline used for the calculation of the rotamerization constant K_r (NAP1)/(NAP2–NAP6).

	Experimental		Calculated		
	Frequency[a] (cm^{-1})	Intensity ($km.mol^{-1}$)	Frequency (cm^{-1})	Intensity ($km.mol^{-1}$)	
NAP1	1616	20.122	1627	353	
NAP2			3566	71	
NAP3			3567	74	
NAP4	3561 + 3547	2.043	3566	71	72[b]
NAP5			3564	73	
NAP6			3561	76	

$K_r = \frac{[(NAP2-NAP6)]}{[NAP1]} = \frac{\left(I_{exp}/I_{theor}\right)_{(NAP2-NAP6)}}{\left(I_{exp}/I_{theor}\right)_{NAP1}} = 0.50$

[a] ν(C═O…)^{ac} for NAP1 and ν(OH) for (NAP2–NAP6).
[b] Theoretical intensity of (NAP2–NAP6) taking into account their abundances at the MP2/6-31++G** level of theory at room temperature.

and γ(OH…). On the other hand, it is difficult to distinguish between the non-H-bonded conformations (NAP2–NAP6), because their frequency differences are small and many bands are superimposed on the bands of NAP1. However, the experimental spectrum demonstrates that at least 2 of these non-H-bonded conformations are present in the matrix, according to the theoretical abundances probably NAP2 and NAP3. The experimental frequency shifts of the H-bonded modes are rather large i.e. ±600 cm^{-1} for Δν(OH), −66 cm^{-1} for ν(C═O)^{ac}, ±300 for δ(OH) and +240 cm^{-1} for γ(OH). The H…O distance in the H-bond OH…O═C (1.733 Å) is small and the OH…O angle is quasi-linear, i.e. 161°, which means that NAP has a strong intramolecular H-bond. This strong intramolecular H-bond explains the large energy gap, for a molecule with such a conformational flexibility as NAP, between NAP1 and the non-H-bonded conformations.

The experimental abundances of 67% for NAP1 and 33% for NAP2–NAP6 are estimated using the experimental intensities of ν(C═O)^{ac} (NAP1) and ν(OH) (NAP2–NAP6) and are in reasonable accordance with the prediction at the sublimation temperature (48% and 52%, respectively).

Compared to proline, NAP has some unique spectral features: not only the expected intense ν(C═O)^{ac} modes at 1616 and 1682 cm^{-1} but also the overtones at 2798 and 2746 cm^{-1} because near these wavenumbers no bands of proline are situated, these features can be used to distinguish between NAP and proline.

The obtained mean frequency deviation between theoretical and experimental frequencies 12.4 or 7.8 cm^{-1} without the ν(OH…) mode, for the assigned modes is typical for DFT frequencies scaled with variable factors. As a matter of fact, the accuracy of the DFT (B3LYP)/6-31++G** frequencies is reasonably good for studying small biomolecules.

Acknowledgments

B. B. acknowledges the Department of Chemistry of the KULeuven for financial support. This research was conducted utilizing the high performance computational resources provided by the University of Leuven, http://ludit.kuleuven.be/hpc.

References

[1] S. Abirami, C.H.-S. Wong, C.W. Tsang, N.L. Ma, N.K. Goh, A theoretical study of potassium cation binding to prolylglycine (PG) and glycylproline (GP) dipeptide, J. Mol. Struct. (THEOCHEM) 729 (2005) 193–202.
[2] A.E. Aliev, S. Bhandal, D. Courtier-Murias, Quantum mechanical and NMR studies of ring puckering and cis/trans-rotameric interconversion in prolines and hydroxyprolines, J. Phys. Chem. A 113 (2009) 10858–10865.
[3] A.E. Aliev, D. Courtier-Murias, Conformational analysis of L-prolines in water, J. Phys. Chem. B 111 (2007) 14034–14042.
[4] A.D. Becke, Density-functional exchange-energy approximation with correct asymptotic-behavior, Phys. Rev. A 38 (1988) 3098–3100.
[5] T. Beke, C. Somlai, G. Magyarfalvi, A. Perczel, G. Tarczay, Chiral and achiral fundamental conformational building units of β-peptides: a matrix isolation conformational study on Ac-β-HGly-NHMe and Ac-β-HAla-NHMe, J. Phys. Chem. B 113 (2009) 7918–7926.
[6] B. Boeckx, R. Ramaekers, G. Maes, A theoretical and matrix-isolation FT-IR investigation of the conformational landscape of N-acetylcysteine, J. Mol. Spectrosc. 261 (2010) 73–81.
[7] Frisch, M.J.T.G.W., Schlegel, H.B., Scuseria, G.E., Robb, M.A., Cheeseman, J.R., Montgomery, Jr.J.A., Vreven, T., Kudin, K., N., Burant, J.C., Millam, J.M., Iyengar, S.S., Tomasi, J., Barone, V., Mennucci, B., Cossi, M., Scalmani, G., Rega, N., Petersson, G.A., Nakatsuji, H., Hada, M., Ehara, M., Toyota, K., Fukuda, R., Hasegawa, J., Ishida, M., Nakajima, T., Honda, Y., Kitao, O., Nakai, H., Klene, M., Li, X., Knox, J.E., Hratchian, H.P., Cross, J.B., Bakken, V., Adamo, C., Jaramillo, J., Gomperts, R., Stratmann, R.E., Yazyev, O., Austin, A.J., Cammi, R., Pomelli, C., Ochterski, J.W., Ayala, P.Y., Morokuma, K., Voth, G.A., Salvador, P., Clifford, S., Cioslowski, J., Stefanov, B.B., Liu, G., Liashenko, A., Piskorz, P., Komaromi, I., Martin, R.L., Fox, D.J., Keith, T., Al-Laham, M.A., Peng, C.Y., Nanayakkara, A., Challacombe, M., Gill, P.M.W., Johnson, B., Chen, W., Wong, M.W., Gonzalez, C., Pople, J.A. Gaussian 03, Revision D.02. 2004. Wallingford CT, Gaussian, Inc. Ref Type: Computer Program
[8] S. Gobi, K. Knapp, E. Vass, Z. Majer, G. Magyarfalvi, M. Hollosi, G. Tarczay, Is [small beta]-homo-proline a pseudo-[gamma]-turn forming element of [small beta]-peptides? An IR and VCD spectroscopic study on Ac-[small beta]-HPro-NHMe in cryogenic matrices and solutions, Phys. Chem. Chem. Phys. 12 (2010) 13603–13615.
[9] A. Gomez-Zavaglia, I.D. Reva, R. Fausto, Matrix-isolation FT-IR spectra and molecular orbital calculations on neutral N,N-dimethylglycine, Phys. Chem. Chem. Phys. 5 (2003) 41–51.
[10] M. Graindourze, J. Smets, T. Zeegers-Huyskens, G. Maes, Fourier transform-infrared spectroscopic study of uracil derivatives and their hydrogen-bonded complexes with proton donors.1. Monomer infrared absorptions of uracil and some methylated uracils in argon matrices, J. Mol. Struct. 222 (1990) 345–364.
[11] Y. Grenie, M. Avignon, C. Garrigou-Lagrange, Molecular-structure study of dipeptides isolated in an argon matrix by infrared spectroscopy, J. Mol. Struct. 24 (1975) 293–307.
[12] A. Kaczor, I.D. Reva, L.M. Proniewicz, R. Fausto, Importance of entropy in the conformational equilibrium of phenylalanine: a matrix-isolation infrared spectroscopy and density functional theory study, J. Phys. Chem. A 110 (2006) 2360–2370.
[13] Y. Kee Kang, H. Sook Park, Ab initio conformational study of N-acetyl-L-proline-N′, N′-dimethylamide: a model for polyproline, Biophys. Chem. 113 (2005) 93–101.
[14] B. Lambie, R. Ramaekers, G. Maes, On the contribution of intramolecular H-bonding entropy to the conformational stability of alanine conformations, Spectrochim. Acta, Part A 59 (2003) 1387–1397.
[15] B. Lambie, R. Ramaekers, G. Maes, Conformational behavior of serine: an experimental matrix-isolation FT-IR and theoretical DFT(B3LYP)/6-31++G** study, J. Phys. Chem. A 108 (2004) 10426–10433.
[16] C.T. Lee, W.T. Yang, R.G. Parr, Development of the Colle–Salvetti correlation-energy formula into a functional of the electron-density, Phys. Rev. B. 37 (1988) 785–789.
[17] C. Moller, M.S. Plesset, Note on an approximation treatment for many-electron systems, Phys. Rev. 46 (1934) 618.
[18] M. Nomura, S. Inouye, Y. Ohmiya, F.I. Tsuji, A C-terminal proline is required for bioluminescence of the Ca2+-binding photoprotein, aequorin, FEBS Lett. 295 (1991) 63–66.
[19] M.A. Palafox, N. Iza, M. de la Fuente, R. Navarro, Simulation of the first hydration shell of nucleosides D4T and thymidine: structures obtained using MP2 and DFT methods, J. Phys. Chem. B 113 (2009) 2458–2476.
[20] G. Pohl, A. Perczel, E. Vass, G. Magyarfalvi, G. Tarczay, A matrix isolation study on Ac-Gly-NHMe and Ac-L-Ala-NHMe, the simplest chiral and achiral building blocks of peptides and proteins, Phys. Chem. Chem. Phys. 9 (2007) 4698–4708.
[21] G. Pohl, A. Perczel, E. Vass, G. Magyarfalvi, G. Tarczay, A matrix isolation study on Ac-l-Pro-NH2: a frequent structural element of [beta]- and [gamma]-turns of peptides and proteins, Tetrahedron 64 (2008) 2126–2133.
[22] R. Ramaekers, A. Dkhissi, L. Adamowicz, G. Maes, Matrix-isolation FT-IR study and theoretical calculations of the hydrogen-bond interaction of hypoxanthine with H2O, J. Phys. Chem. A 106 (2002) 4502–4512.
[23] R. Ramaekers, J. Pajak, B. Lambie, G. Maes, Neutral and zwitterionic glycine.H_2O complexes: a theoretical and matrix-isolation Fourier transform infrared study, J. Chem. Phys. 120 (2004) 4182–4193.
[24] R. Ramaekers, J. Pajak, G. Maes, On the intramolecular H-bond entropy contribution to the stability of glycine conformations, Asian Chem. Lett. 2 & 3 (2004) 203–209.

[25] H. Rostkowska, L. Lapinski, M.J. Nowak, Analysis of the normal modes of molecules with D-3h symmetry Infrared spectra of monomeric s-triazine and cyanuric acid, Vib. Spectrosc. 49 (2009) 43–51.
[26] O.E. Schroeder, E. Carper, J.J. Wind, J.L. Poutsma, F.A. Etzkorn, J.C. Poutsma, Theoretical and experimental investigation of the energetics of cis/trans proline isomerization in peptide models, J. Phys. Chem. A 110 (2006) 6522–6530.
[27] I.Z. Siemion, T. Wieland, K.H. Pook, Influence of distance of proline carbonyl from beta and gamma carbon on C-13 chemical-shifts, Angewandte Chemie-International Edition in English 14 (1975) 702–703.
[28] S.G. Stepanian, I.D. Reva, E.D. Radchenko, L. Adamowicz, Conformers of nonionized proline. Matrix-isolation infrared and post-Hartree-Fock ab initio study, J. Phys. Chem. A 105 (2001) 10664–10672.
[29] M.K. VanBael, J. Smets, K. Schoone, L. Houben, W. McCarthy, L. Adamowicz, M.J. Nowak, G. Maes, Matrix-isolation FTIR studies and theoretical calculations of hydrogen-bonded complexes of imidazole. A comparison between experimental results and different calculation methods, J. Phys. Chem. A 101 (1997) 2397–2413.
[30] C. Venien-Bryan, A. Davies, K. Langmack, J. Baverstock, A. Watts, D. Marsh, H. Saibil, Effect of the C-terminal proline repeats on ordered packing of squid rhodopsin and its mobility in membranes, FEBS Lett. 359 (1995) 45–49.
[31] D.E. Warnock, L.J. Terlecky, S.L. Schmid, Dynamin GTPase is stimulated by crosslinking through the C-terminal proline-rich domain, EMBO J. 14 (1995) 1322–1328.